Journal of Alloys and Compounds 489 (2010) 685–688

Contents lists available at ScienceDirect

Journal of Alloys and Compounds

journal homepage: www.elsevier.com/locate/jallcom

Correlation between microhardness and electronic charge density of hafnium hydrides

B. Tsuchiya*, R. Sahara, M. Oku, K. Konashi, S. Nagata, T. Shikama, H. Mizuseki, Y. Kawazoe

Institute for Materials Research, Tohoku University, 2-1-1, Katahira, Aoba-ku, Sendai, Miyagi 980-8577, Japan

ARTICLE INFO

Article history:
Received 1 September 2008
Accepted 23 September 2009
Available online 2 October 2009

PACS:
62.20.−x
71.20.−b

Keywords:
Hafnium hydride
Vickers microhardness
Electronic structure
Charge transfer

ABSTRACT

Quantitative Vickers microhardnesses for α + δ′-, δ′-, δ-, δ + ε- and ε-phase hafnium hydrides (HfH_x; $1.46 \le x \le 2.02$) and deuterides (HfD_x; $1.55 \le x \le 1.94$) at room temperature have been measured using a Vickers hardness tester. The Vickers microhardnesses of the HfH_x and HfD_x gradually decreased with an increase of the hydrogen concentration, and those for $1.46 \le x \le 1.70$ were higher than that of α-phase metallic Hf. It was revealed by a first-principles calculation as well as an X-ray photoelectron spectroscopy (XPS) measurement that the hydrogen concentration dependence of the microhardnesses for HfH_x and HfD_x was ascribed mainly in terms of its influence on charge transfer from Hf 5*d* to H 1*s* and reduction of cohesive energy.

1. Introduction

The hafnium hydrides (HfH_x) or deuterides (HfD_x) have a potential as ones of new candidate materials of control rods for the fast neutron flux process in fast reactors [1]. For the fast neutron absorption process to HfH_x and HfD_x rods, the thermal neutrons, generated by elastic collisions of the fast neutrons with hydrogen isotope atoms, are absorbed by Hf atoms. On the other hand, it is predicted that the compositions in the HfH_x and HfD_x rods are changed by the elastic collisions with fast neutrons as well as temperature elevations due to gamma-heating effects, and in addition the concentration gradient of the hydrogen isotopes is caused at the parts of center and edge inside the rods. In order to design these hydride and deuteride control rods, it is extremely important to understand changes in the physical, chemical, thermal and mechanical properties of the hydrides and deuterides relative to the hydrogen isotope distributions within the rod itself.

At this time, there is a scarcity of reported data concerning Vickers microhardness, which is one of the most important parameters regarding the mechanical properties, of HfH_x and HfD_x with various hydrogen isotope concentrations. In the present study, the objectives were to obtain quantitative Vickers microhardness at room temperature for HfH_x and HfD_x against the composition using Vickers hardness tester, and evaluate the hydrogen concentration dependence of the mechanical property by taking into account electronic structure which was not only measured on the surface fractured in ultrahigh vacuum using a X-ray photoelectron spectroscopy (XPS) and but also simulated using a first-principles calculation.

2. Experimental

HfH_x ($1.46 \le x \le 2.02$) or HfD_x ($1.55 \le x \le 1.94$) compounds were prepared with a Sieverts apparatus by heating and outgassing hafnium pure metal (99.8% quality) with the dimensions of $\varnothing 10 \times 1.0\,mm^3$ in an evacuated quartz tube at 1073 K, followed by exposure to 99.9% pure hydrogen or deuterium gases in the tube at pressures ranging from 0.1 to 1.0×10^5 Pa for 4 h. The specimens were then cooled to room temperature at a rate of 4.5×10^{-3} K/s while still in the tube. The compositions of the specimens were calculated based on mass gain after the hydrogenation.

X-ray diffraction (XRD) measurements confirmed that the hafnium–hydrogen system at room temperature consists of three phases and the presence of mixtures. The crystal structures of the compositions with $1.60 \le x \le 1.73$ and $1.84 \le x \le 2.02$ were face-centered cubic (fcc) δ-phase and face-centered tetragonal (fct) ε-phase, respectively [2–4]. The HfH_x or HfD_x specimens with $1.74 \le x \le 1.83$ had δ + ε-phase structures that were mixtures of a δ-phase with a ε-phase. The crystal structures of the composition with $1.48 \le x \le 1.59$ were distinguishable from the δ-phase structure by the XRD patterns, and exhibited a pseudocubic defect δ-phase (δ′-phase) that has previously been reported in other literature [4–6]. The unit cell of this pseudocubic phase is slightly deformed and displays some tetragonal characteristics, such as the lattice constants for the *a* and *b* axes having the same values as those of the δ-phase, while that for the *c* axis is lower. The HfH_x or HfD_x specimens with $1.46 \le x \le 1.47$ had α + δ′-phase structures consisting of a mixture of a hexagonal α-phase and a δ′-phase [4]. It has been reported in the literature [3] that the hydrogen atoms in the ε- and δ-phases are located in vacant tetrahedral interstices.

* Corresponding author. Tel.: +81 22 215 2063; fax: +81 22 215 2061.
E-mail address: tsuchiya@imr.tohoku.ac.jp (B. Tsuchiya).

0925-8388/$ – see front matter © 2009 Elsevier B.V. All rights reserved.
doi:10.1016/j.jallcom.2009.09.151

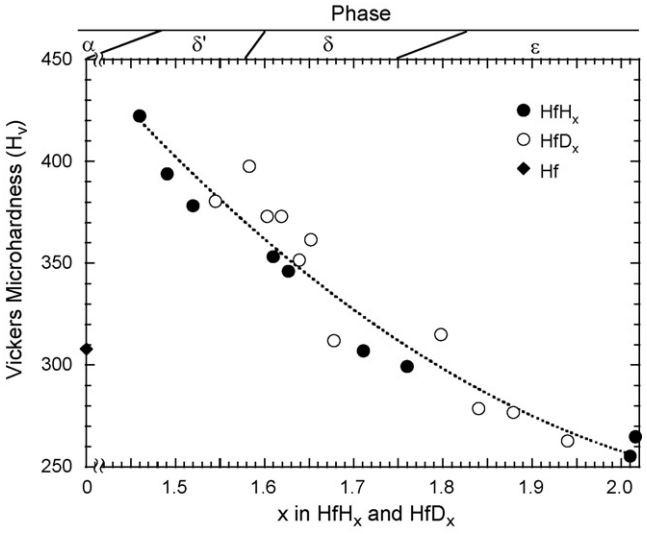

Fig. 1. Vickers microhardnesses of HfH_x ($1.46 \le x \le 2.02$) and HfD_x ($1.55 \le x \le 1.94$), measured at room temperature.

The Vickers microhardness measurement for the estimation of the mechanical property of the HfH_x or HfD_x specimens prepared was carried out at room temperature in air using the Vickers hardness tester. The diagonal length of the impression, produced under a load of 0.1 kg by a pyramid-shaped diamond indenter, was ≤26 μm and less than the average grain size of approximately ϕ 100 μm. To investigate the electronic structure of the hydride bulk, the surface of the hydride specimen fractured in ultrahigh vacuum was observed in situ using XPS with K-α X-rays of 1486.6 eV from an aluminum target [7]. The electronic structure of Hf metal was also observed after it was sputtered with 2 keV Ar^+ ions in order to remove surface impurities, since it is extremely difficult for metals to fracture its surface. In addition, first-principles calculations were performed to estimate the density of states (DOS) and cohesive energy for hexagonal Hf (α-phase), deformed cubic $HfH_{1.50}$ (δ′-phase), δ-phase cubic $HfH_{1.75}$ (δ-phase), and tetragonal $HfH_{2.00}$ (ε-phase). In the calculation, the effect of crystal-structural change on the electronic structure was considered using the projected augmented wave method with the Vienna *ab initio* simulation package (VASP) [8–10]. The exchange-correlation energy was calculated within the generalized gradient approximation (GGA) [11]. The cut-off energy for the plane wave expansion was taken to be 584.6 eV. For Brillouin zone integrations, we use $8 \times 8 \times 8$ **k**-points. In order to describe substoichiometric concentrations, appropriate H atoms positioned at tetrahedral sites are replaced by vacancies. The atomic positions and structural parameters are fully optimized by the conjugated gradient method for δ′-phase $HfH_{1.53}$, δ-phase $HfH_{1.76}$, and ε-phase $HfH_{2.00}$, using the lattice parameters measured at room temperature as the initial condition [4,12].

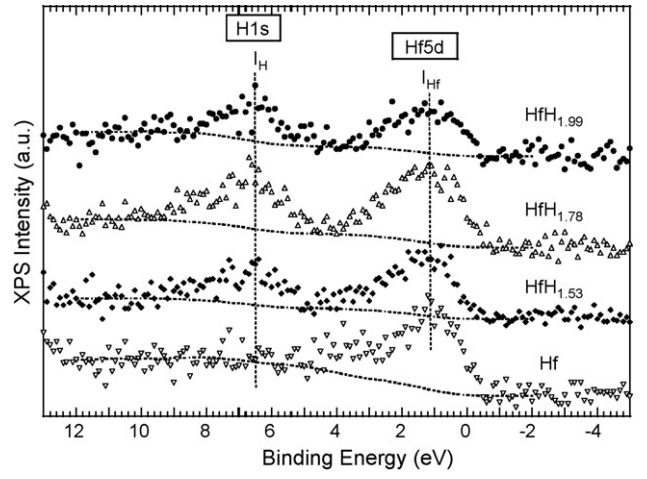

Fig. 2. Valence band photoelectron spectra for the fractured surfaces of δ′-$HfH_{1.53}$, δ + ε-$HfH_{1.78}$, and ε-$HfH_{1.99}$, as compared with the Ar^+ ion-sputtered surface of α-Hf.

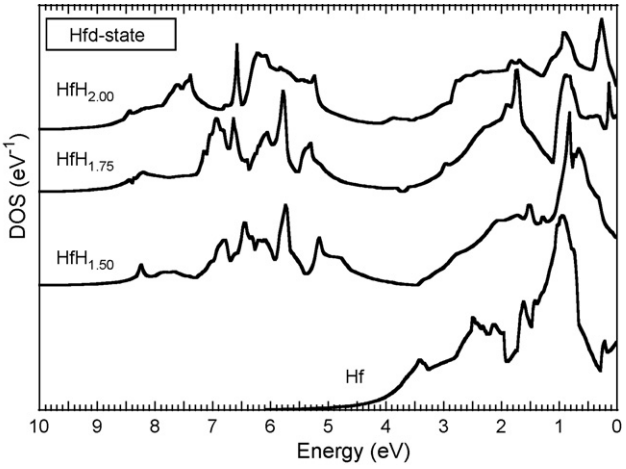

Fig. 3. DOS spectra of *d* band state in the valence bands for α-Hf, δ′-$HfH_{1.50}$, δ-$HfH_{1.75}$, and ε-$HfH_{2.00}$.

3. Experimental results and discussion

Fig. 1 shows the Vickers microhardnesses of (●) HfH_x ($1.46 \le x \le 2.02$), (○) HfD_x ($1.55 \le x \le 1.94$), and (♦) α-Hf, respectively, which are measured at room temperature using the Vickers hardness tester. The dashed curve in Fig. 1 represents the empirical values of the microhardnesses H_v of HfH_x and HfD_x, which can be expressed as a function of composition x as follows; $H_v = 1.70 \times 10^3 - 1.30 \times 10^3 x + 2.88 \times 10^2 x^2$. The both microhardnesses of HfH_x and HfD_x decrease as the compositions increase, and, for HfH_x and HfD_x ($x > 1.76$) according to the equation above, the microhardnesses are lower than that of α-Hf. In addition, the microhardness of HfH_x is similar to those of HfD_x. The experimental result indicates no isotope effect on the microhardness for the composition region of $1.46 \le x \le 2.02$, and the effect of electronic density between Hf and H (or D).

The electronic structures of the bulk of δ′-$HfH_{1.53}$, δ + ε-$HfH_{1.78}$, and ε-$HfH_{1.99}$, fractured in ultrahigh vacuum, were observed in situ in O 1*s* and C 1*s* core energy and valence band levels using XPS. The electronic structure of the Ar^+ ion-sputtered surface of α-Hf is also observed. While oxygen and carbon are scarce on the topmost fractured surface of HfH_x, they remain on its sputtered surface of α-Hf. Their contaminations cannot be completely removed. Fig. 2 shows the XPS spectra in the valence bands, including the Hf 5*d* band at 1.1 ± 0.1 eV and a new band at 6.5 ± 0.1 eV below the Fermi level for α-Hf, δ′-$HfH_{1.53}$, δ + ε-$HfH_{1.78}$, and ε-$HfH_{1.99}$. The new photo-

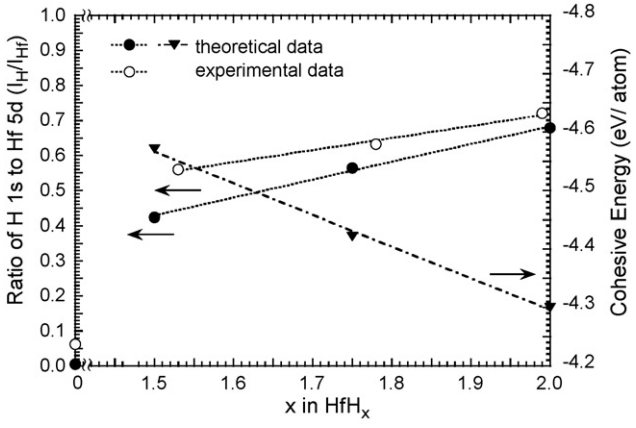

Fig. 4. Composition dependences on the ratios (I_H/I_{Hf}) of a new peak area (I_H, 5–8 eV) to the Hf 5*d* photoelectron peak area (I_{Hf}, 0–3 eV), and the cohesive energies.

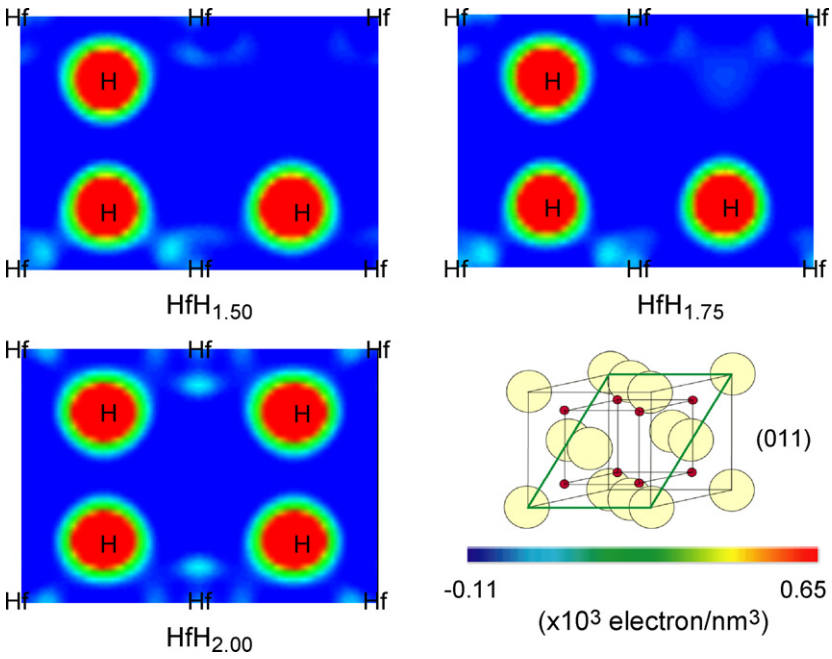

Fig. 5. Electronic charge densities for (0 1 1) plane of δ′-$HfH_{1.50}$, δ-$HfH_{1.75}$, and ε-$HfH_{2.00}$ at temperature of 0 K.

electron peaks as well as 5*d* ones for δ′-$HfH_{1.53}$, δ + ε-$HfH_{1.78}$, and ε-$HfH_{1.99}$ are broad, and show no significant change for the binding energy in the presences of hydrogen atoms in the interstices. Further, the new peak is also broad, and reveals no significant change in the presence of hydrogen and deuterium atoms interstitials.

To understand the presence of the new peak in the valence band and the change in the intensities of the new and 5*d* photoelectron peaks, the site-projected DOS of the *d* state of Hf for α-Hf, δ′-$HfH_{1.50}$, δ-$HfH_{1.75}$, and ε-$HfH_{2.00}$ obtained by first-principles calculations are shown in Fig. 3. The intensity of DOS represents the charge of electrons per energy level in *d* band states. It can be seen in Fig. 3 that some new peaks in the energy region of 5.0–8.0 eV for δ′-$HfH_{1.50}$, δ-$HfH_{1.75}$, and ε-$HfH_{2.00}$, are shown by adding H. Moreover, a clear chemical shift to lower energy of Hf 5*d* peaks is revealed for HfH_x, as compared with that for α-Hf. The DOS of the energy level of H 1*s* band were also calculated. The energy level was measured at approximately 5.0–9.0 eV. The appearance of the new state may indicate hybrid orbitals comprising H 1*s* and Hf 5*d* states. The ratios (I_H/I_{Hf}) of the intensity of a new peak (I_H) to that of the Hf 5*d* photoelectron peak (I_{Hf}) at binding energies of 5.0–8.0 and 0–3.0 eV, respectively, are shown as a function of the hydrogen content in Fig. 4. The experimental results are also plotted; these results are obtained by subtracting the background, calculated using Shirley method, from the intensities at 5.0–8.0 and 0–3.0 eV in Fig. 2. The experimental and theoretical values of I_H/I_{Hf} increase with an increase in the hydrogen content, although their absolute values are different each other. These results are in agreement with the experimental and theoretical data for TiH_x and TiD_x which have been reported in the literatures [7,13].

In order to further check the bonding character, Fig. 5 shows the electronic charge densities for (0 1 1) plane of δ′-$HfH_{1.50}$, δ-$HfH_{1.75}$, and ε-$HfH_{2.00}$ obtained by the calculation. It is shown in Fig. 5 that the charge density at each H site is significantly higher than that at Hf sites. The result shows that the hybrid orbitals comprising H 1*s* and Hf 5*d* band states are formed around H atoms. The charge density around Hf sites decreases with increasing the H contents. This result supports the theory that charge transfer from Hf 5*d* to H 1*s* is caused by the presence of hydrogen atoms, and leads to reduction of charge density between Hf and Hf atoms. Moreover, the cohesive energies E_c that are required to break all the bonds such as Hf–H, H–H, and Hf–Hf associated with one of its constituent solids, also decrease with increasing the H content, as shown in Fig. 4. The values of E_c are obtained simultaneously from the expression $E_c = E_{HfH_x} - (E_{Hf} + xE_H)$ using the first-principles calculation. Therefore, the reduction of the electronic charge density between Hf and Hf with an increase of hydrogen atoms significantly leads to the decrements of E_c, and may affect on the mechanical properties.

4. Summary

The Vickers microhardness which is one of the most important parameters regarding the mechanical property, of HfH_x ($1.46 \le x \le 2.02$) and HfD_x ($1.55 \le x \le 1.94$) prepared by adjusting the temperature and hydrogen gas pressure with a Sieverts apparatus, at room temperature was measured using Vickers hardness tester. The hydrogen concentration dependence of the mechanical properties was evaluated by taking into account the electronic structure which is not only measured on the surface fractured in ultrahigh vacuum using XPS but also simulated using a first-principles calculation.

The Vickers microhardness of the α + δ′-, δ′-, δ-, δ + ε- and ε-phase HfH_x and HfD_x gradually reduced with increase of the hydrogen concentration. In XPS spectra for valence band of δ′-$HfH_{1.53}$, δ + ε-$HfH_{1.78}$, and ε-$HfH_{1.99}$, a new peak associated with hybridized orbitals of H 1*s* and Hf 5*d* appeared at a binding energy of around 6.5 eV. The ratio of the new peak to the Hf 5*d* peak increased with an increase in the hydrogen concentration. The experimental result can be interpreted by the first-principles calculation that the decreases of DOS at Hf 5*d* energy level by charge transfer from Hf 5*d* to H 1*s* lead to reduction of cohesive energy of $HfH_{1.50-2.00}$. The hydrogen concentration dependence of the mechanical property for HfH_x and HfD_x ($x \ge 1.5$) is concluded mainly in terms of its influence on charge transfer from Hf 5*d* to H 1*s* that results from changing the hydrogen concentration.

References

[1] K. Konashi, et al., Development of advanced control rod of hydride hafnium for fast reactor, in: Proc. ICAPP'06, Reno, USA, 2006.
[2] S.S. Sidhu, Acta Cryst. 7 (1954) 447.

[3] S.S. Sidhu, L. Heaton, D.D. Zauberis, Acta Cryst. 9 (1956) 607.
[4] S.S. Sidhu, J.C. McGuire, J. Appl. Phys. 23 (11) (1952) 1257.
[5] L. Espagno, P. Azou, P. Bastien, Compt. Rend. 250 (1960) 4352.
[6] R.K. Edwards, E. Veleckis, J. Phys. Chem. 66 (1962) 1657.
[7] B. Tsuchiya, M. Oku, R. Sahara, S. Nagata, T. Shikama, Y. Kawazoe, J. Surf. Anal. 14 (4) (2008) 424.
[8] G. Kresse, D. Joubert, Phys. Rev. B 59 (1999) 1758.
[9] D. Vanderbilt, Phys. Rev. B 41 (1990) 7892.
[10] G. Kresse, J. Hafner, Phys. Rev. B 47 (1993) 558.
[11] J.P. Perdew, Y. Wand, Phys. Rev. B 45 (1992) 13244.
[12] M.H. Mintz, Hydrogen Metal Systems I, Chapter 8, Hafnium–Hydrogen, 1996, p. 331.
[13] B.C. Lamartine, T.W. Haas, J.S. Solomon, Appl. Surf. Sci. 4 (1980) 537.